A State-Space EMG Model for the Estimation of Continuous Joint Movements

Jianda Han, *Member, IEEE*, Qichuan Ding, Anbin Xiong, and Xingang Zhao, *Member, IEEE*

***Abstract*—A state-space electromyography (EMG) model is developed for continuous motion estimation of human limb in this paper. While the general Hill-based muscle model (HMM) estimates only joint torque from EMG signals in an "open-loop" form, we integrate the forward dynamics of human joint movement into the HMM, and such an extended HMM can be used to estimate the joint motion states directly. EMG features are developed to construct measurement equations for the extended HMM to form a state-space model. With the state-space HMM, a normal closed-loop prediction–correction approach such as the Kalman-type algorithm can be used to estimate the continuous joint movement from EMG signals, where the measurement equation is used to reject model uncertainties and external disturbances. Moreover, we propose a new normalization approach for EMG signals for the purpose of rejecting the dependence of the motion estimation on varying external loads. Comprehensive experiments are conducted on the human elbow joint, and the improvements of the proposed methods are verified by the comparison of the EMG-based estimation and the inertial measurement unit measurements.**

***Index Terms*—Closed-loop estimation, continuous joint motion, electromyography (EMG), muscle model.**

I. Introduction

USING ELECTROMYOGRAPHY (EMG) as control signals to realize a "friendly" human–robot interface (HRI) has been there for assistive robots [1]–[3]. Classification, which distinguishes different patterns of motion from EMG, is one of the key techniques for such an HRI [4]. The classification involves two steps: 1) extracting feature sets from EMG and 2) classifying different motions based on the selected feature sets [5]. For step 1, the EMG feature sets include EMG amplitude, autoregressive coefficients, waveform length, cepstrum coefficients, and the wavelet packet transform [6]. Certain feature sets, such as the wavelet packet transform, have to be used in conjunction with dimension reduction algorithms such as principal components analysis [7] or linear discriminant analysis [8] to yield proper signal representation. For step 2, commonly used classification algorithms are support vector machine [9], artificial neural networks [10], hidden Markov model [11], Gaussian mixture model [12], and neuro-fuzzy algorithm [13].

The aforementioned algorithms are able to identify a limited number of discrete motion patterns from EMG. However, recently, instead of the discrete patterns, how to determine the human's intent of a continuous motion from EMG has become an active issue. This is due to the requirements of several possible applications, such as powered prosthesis, exoskeletons, and rehabilitative robots [14], [15]. In such a system, the human motion intents have to be continuously recognized from EMG and further reconstructed as control commands to a robotic device, so that the robot could match the human's intent and then perform efficient assistance.

Involving a physiological muscle model into classification algorithm is a way to achieve continuous EMG recognition, and the Hill-based muscle model (HMM) is the most frequently utilized one [16]–[19]. In [16], an EMG-based forward dynamics model was proposed, which consists of muscle activation dynamics, Hill-based muscle contraction dynamics, musculoskeletal geometry, and joint forward dynamics. This model is very complex and involves many unknown physiological parameters, which limits its applications in real mechatronic systems. A simplified model for controlling lower extremity exoskeleton was developed in [18], where a step calibration process was constructed to optimize the estimation of unknown parameters.

However, there exist two problems while the normal Hill-type models are used to estimate continuous motion states of human limbs. First, a full Hill model always involves many physiological parameters, which are very difficult to be accurately identified. The complex model will also introduce extra computational burden. Thus, a simplified model is often used for real-time applications. However, a simplified model inherently has modeling errors that will degrade the estimation accuracy. Normally, the measurement equations in a state-space model will reduce the effects of modeling errors and uncertainties. However, the Hill-type models are in "open-loop" structure; there are no other measurement equations that can be used as a kind of feedback to improve the estimation accuracy.

Second, the Hill-type models are often used to directly calculate the joint torque from EMG signals [18]–[21]. For the applications where the continuous estimations of human joint are required, for example, to control a robotic device assisting the movement of human limb [22], we have to further calculate the motion states, such as angular velocity and position, from

Manuscript received February 15, 2014; revised June 11, 2014 and October 4, 2014; accepted November 7, 2014. Date of publication January 1, 2015; date of current version May 15, 2015. This work was supported in part by the National Natural Science Foundation of China under Grant 61273355, Grant 61273356, and Grant 61035005.

J. Han and X. Zhao are with the State Key Laboratory of Robotics, Shenyang Institute of Automation, Chinese Academy of Sciences, Shenyang 110016, China (e-mail: jdhan@sia.cn).

Q. Ding and A. Xiong are with the State Key Laboratory of Robotics, Shenyang Institute of Automation, Chinese Academy of Sciences, Shenyang 110016, China, and also with the University of the Chinese Academy of Sciences, Beijing 100049, China.

Color versions of one or more of the figures in this paper are available online at http://ieeexplore.ieee.org.

Digital Object Identifier 10.1109/TIE.2014.2387337

the EMG-recognized torque indirectly. This usually introduces accumulated errors into the estimated joint motion states and further worsens the estimation accuracy.

With respect to the preceding two problems, in this paper, we first developed a model that brings together the HMM and the joint forward dynamics. Instead of joint torque, this model can be used to calculate the joint motion from EMG directly. Then, two EMG features are proposed to construct measurement equations, and a state-space model is derived for continuous motion state estimation. Moreover, a new normalization approach for EMG signals is also proposed in order to reduce the dependence of the motion state estimation on different external loads of human limb.

Extensive experiments were conducted to validate the performance of the proposed methods. In our experiments, the proposed method was applied to estimate the angular velocity and position of a human elbow joint from the EMG signals measured by surface electrodes that were placed on the biceps brachii. An inertial measurement unit (IMU) was also attached to the human forearm to actually measure the elbow joint movements and used as a reference to verify the estimations. All the results of the EMG-model-based estimations were compared with the IMU measurements, to demonstrate the validity and improvements of the proposed methods.

II. HMM

Here, we briefly introduce the HMM as the basis of the proposed approach.

A. EMG Signal to Muscle Activation

Muscle activation reflects the level of the active force produced by the muscle. First, raw EMG signals need to be preprocessed by high-pass filtering, full-wave rectification, low-pass filtering, and then normalized with respect to the muscle's maximum voluntary contraction (MVC) level [16], [20]. We use $e(k)$ to present the preprocessed EMG signal at time k. A recursive filter is used to calculate the neural activation from the normalized signal [16], [20], i.e.,

$$u(k) = \alpha \cdot e(k - d/T_{\text{emg}}) - \beta_1 \cdot u(k-1) - \beta_2 \cdot u(k-2) \quad (1)$$

where $u(k)$ is the neural activation at time k; d is the electromechanical delay, and normally, $d = 40$ ms [16]; T_{emg} is the sampling time of EMG signal; and α, β_1, and β_2 are coefficients that define the second-order dynamics.

To realize a positive stable solution, a set of constraints has to be employed [16], [20], i.e.,

$$\beta_1 = \gamma_1 + \gamma_2 \quad \beta_2 = \gamma_1 \cdot \gamma_2, \qquad \alpha - \beta_1 - \beta_2 = 1 \quad (2)$$

where $|\gamma_1| < 1$, and $|\gamma_2| < 1$.

The relationship between neural activation $u(k)$ and muscle activation $a(k)$ was proposed in [21], i.e.,

$$a(k) = \frac{e^{A \cdot u(k)} - 1}{e^A - 1} \quad (3)$$

where A is a factor varying between -3 and 0.

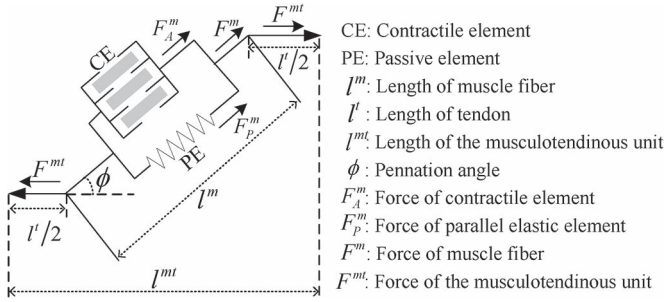

Fig. 1. HMM.

B. Muscle Activation to Generated Torque

HMM consists of two elements: a contractile element producing the active muscle force F_A^m and a parallel elastic element producing the passive force F_P^m. Fig. 1 shows the schematic of muscle–tendon and the muscle fiber with the contractile element and parallel elastic component [18]. The model can be described as [16], [18], [19]

$$\begin{cases} F_A^m = f_A(l) \cdot f_V(v) \cdot a(k) \cdot F_0^m \\ F_P^m = f_P(l) \cdot F_0^m \end{cases}$$

where $f_A(l)$, $f_V(v)$, and $f_P(l)$ define the normalized active force–length relationship, the force–velocity relationship, and the passive elastic force–length relationship, respectively; F_0^m is the maximum isometric muscle force; $a(k)$ is the muscle activation; l is the normalized muscle fiber length, v is the normalized muscle fiber velocity, and

$$l = l^m / l_0^m \quad v = v^m / v_0^m \quad (4)$$

where l^m and v^m are the fiber length and the muscle contraction velocity, respectively; l_0^m represents the optimal fiber length; and v_0^m is the maximum muscle contraction velocity.

Furthermore, the musculotendon force F^{mt} can be calculated as [16], [19]

$$\begin{aligned} F^{\text{mt}} &= [F_A^m + F_P^m] \cdot \cos(\phi) \\ &= [f_A(l) \cdot f_V(v) \cdot a(k) + f_P(l)] \cdot F_0^m \cdot \cos(\phi) \end{aligned} \quad (5)$$

where ϕ is the pennation angle.

In order to calculate (5), some simplifications have been already proposed to replace the complex biomechanical parameters [16], [18], [23], [24], i.e.,

$$f_A(l) = \begin{cases} q_0 + q_1 \cdot l + q_2 \cdot l^2, & 0.5 \le l \le 1.5 \\ 0, & \text{otherwise} \end{cases} \quad (6a)$$

$$f_P(l) = e^{10 \cdot l - 15} \quad (6b)$$

$$f_V(v) = = 1 \quad (6c)$$

where $q_0 = -2.06$, $q_1 = 6.16$, and $q_2 = -3.13$ are set to be constants, according to the force–length curve fitting algorithm depicted in [21], [23], and [24].

According to Fig. 1, the musculotendon length l^{mt} can be calculated as

$$l^{\text{mt}} = l^t + l^m \cdot \cos(\phi) \quad (7)$$

where l^t is the total length of the tendons.

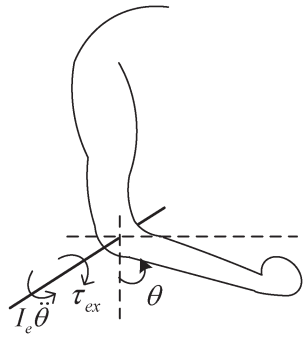

Fig. 2. Movement of elbow joint.

The physiological parameters of $(F_0^m, l^t, l_0^m, \phi)$ can be also set as constants [16], [24]–[26]. Thus, once the musculotendon length of l^{mt} and the constants of $(F_0^m, l^t, l_0^m, \phi)$ are known, we could calculate l^m by (7), l by (4), and, finally, calculate the musculotendon force by (5).

In addition to (7), the musculotendonous length of l^{mt} can be also simplified by a polynomial of the joint angle normally [16], [27], [28]. In this paper, we only use a first-order polynomial to express it, i.e.,

$$l^{\mathrm{mt}} = b_0 + b_1 \cdot \theta \tag{8}$$

where θ is the joint angle, and b_0 and b_1 are constants. In this paper, we use the biceps brachii and the elbow joint shown in Fig. 2 as an example to do all the experiments. Then, the moment arm r can be calculated using the tendon displacement method described in [25], i.e.,

$$r = \frac{\partial l^{\mathrm{mt}}(\theta)}{\partial \theta} = b_1. \tag{9}$$

Thus, the muscle's contribution to the joint moment is

$$\tau = F^{\mathrm{mt}} \cdot r \tag{10}$$

where τ is the joint moment.

III. State-Space Joint Motion Model

Here, we derive the EMG-driven model that directly maps the EMG signals to the joint motion states by integrating the joint forward dynamics into the HMM and the measurement equation by EMG features. Without losing the generality, we also use the elbow joint as an example. It should be noted that the procedure will be the same for another muscle and the joint it actuates.

A. EMG-Driven Joint Motion Model

As shown in Fig. 2, the angular acceleration of the elbow joint can be calculated using the joint forward dynamics, i.e.,

$$\ddot{\theta} = \frac{1}{I_e} \cdot (\tau - \tau_{\mathrm{ex}}). \tag{11}$$

$$\tau_{\mathrm{ex}} = \tau_{\mathrm{ex\_max}} \cdot \sin(\theta) \tag{12}$$

where I_e is the moment of inertia of the forearm about the elbow joint, which is assumed to be constant for a fixed external load, τ_{ex} is a combination of the external torque and the forearm gravity torque, and $\tau_{\mathrm{ex\_max}}$ is the maximum value of τ_{ex}.

Combining the modified Hill-based model with the joint forward dynamics, i.e., substituting (4)–(10) and (12) into (11), we have

$$\ddot{\theta} = (s_0 + s_1 \cdot \theta + s_2 \cdot \theta^2) \cdot a(k) + s_3 \cdot e^{s_4 \cdot \theta} - s_5 \cdot \sin(\theta) \tag{13}$$

where $s_i (i = 0, 1, \ldots, 5)$ are constants given in the following:

$$\begin{cases} s_0 = \frac{k_0 \cdot F_0^m \cdot b_1 \cdot \cos\phi}{I_e} + \frac{k_1 \cdot F_0^m \cdot (b_0 - l^t) \cdot b_1}{l_0^m \cdot I_e} \\ \qquad + \frac{k_2 \cdot F_0^m \cdot (b_0 - l^t)^2 \cdot b_1}{(l_0^m)^2 \cdot I_e \cdot \cos\phi} \\ s_1 = \frac{k_1 \cdot F_0^m \cdot (b_1)^2}{l_0^m \cdot I_e} + \frac{2 \cdot k_2 \cdot (b_0 - l^t) \cdot (b_1)^2}{(l_0^m)^2 \cdot I_e \cdot \cos\phi} \\ s_2 = \frac{k_2 \cdot F_0^m \cdot (b_1)^3}{(l_0^m)^2 \cdot I_e \cdot \cos\phi} \\ s_3 = \frac{F_0^m \cdot b_1 \cdot \cos\phi}{I_e} \cdot \exp\left(\frac{10 \cdot (b_0 - l^t)}{l_0^m \cdot \cos\phi} - 15\right) \\ s_4 = \frac{10 \cdot b_1}{l_0^m \cdot \cos\phi}, \quad s_5 = \frac{\tau_{\mathrm{ex\_max}}}{I_e}. \end{cases}$$

Consequently, we get the EMG-driven joint motion model in discrete time, i.e.,

$$\begin{cases} \ddot{\theta}_{k+1} = \left(s_0 + s_1 \cdot \theta_k + s_2 \cdot \theta_k^2\right) \cdot a(k) \\ \qquad + s_3 \cdot e^{s_4 \cdot \theta_k} - s_5 \cdot \sin(\theta_k) \\ \dot{\theta}_{k+1} = \dot{\theta}_k + \ddot{\theta}_k \cdot T_s \\ \theta_{k+1} = \theta_k + \dot{\theta}_k \cdot T_s \end{cases} \tag{14}$$

where T_s is the sampling time; and $\dot{\theta}_k$ and θ_k are the joint angular velocity and position at time k, respectively.

B. EMG Features and State-Space Model

Equation (14) presents a simplified model that describes the relationship between the EMG signal of $a(k)$ and the joint motion state of θ_k, i.e., an open-loop model. The parameters of s_i in (14) can be identified by offline EMG data and stored as constant coefficients for real-time application, whereas the joint motion states can be directly calculated by (14) using the real-time EMG signal of $a(k)$.

However, it is only an assumption that the parameters of s_i are constants. Indeed, (14) involves uncertainties caused by the following two issues: 1) the derivation of (14) has omitted some physiological parameters for simplification; and 2) the biomechanical parameters involved in s_i are subject dependent and can change due to varying conditions of the skin and body state. The unmodeled uncertainties can result into errors in the calculation of joint motion states. Even worse, the errors will accumulate during the recursive calculation of (14).

In order to eliminate the errors due to the unmodeled uncertainties, we try to provide a "measure equation" to (14) and form a state-space EMG model. Because there are no other sensors on the human limb in addition to the EMG electrodes that could provide the joint motion measurements as a feedback, we propose to employ the EMG features to construct a state-space EMG model.

In addition to the muscle activation $a(k)$ of EMG signal, there exist other features of EMG that are not employed in (14), such as amplitude, waveform length, and cepstrum coefficients, which might be useful to further improve the estimation accuracy of the joint motion. Here, we propose to build the measurement equation by two EMG features, i.e., waveform length (*WL*) and zero crossing (*ZC*).

Let ξ_i be the ith sample of raw EMG signals and N be the size of a time window. Thus,

$$N = T_{\text{win}}/T_{\text{emg}} \tag{15}$$

where T_{win} and T_{emg} are the time window length and the sampling time of EMG signal, respectively,

$$\text{WL} = \sum_{i=1}^{N-1} |\xi_{i+1} - \xi_i| \tag{16}$$

$$\text{ZC} = \sum_{i=1}^{N-1} \text{sgn}(-\xi_i \cdot \xi_{i+1}) \quad \text{sgn}(\mu) = \begin{cases} 1, \text{ if } \mu > 0 \\ 0, \text{otherwise} \end{cases} \tag{17}$$

where $\text{sgn}(\cdot)$ denotes the sign function.

In what follows, we propose to use the following two second-order polynomials as "fitting functions" to relate the EMG features with the joint movement:

$$y_k^j = c_0^j + c_1^j \cdot \dot{\theta}_k + c_2^j \cdot \theta_k + c_3^j \cdot \dot{\theta}_k^2 + c_4^j \cdot \theta_k^2 + c_5^j \cdot \dot{\theta}_k \cdot \theta_k \tag{18}$$

where $j = 1, 2$; y_k^1 and y_k^2 represent the WL and ZC of EMG signals at time k, respectively, i.e.,

$$\begin{cases} y_k^1 = \text{WL}(k) \\ y_k^2 = \text{ZC}(k) \end{cases}$$

and c_i^j $(i = 0, 1, \ldots, 5)$ are defined as constant parameters, which need to be identified offline.

Combining (14) and (18), we obtain a nonlinear expression in a general form, i.e.,

$$\begin{cases} x_{k+1} = f(x_k, a_k) + \omega_k \\ y_{k+1} = h(x_{k+1}) + \upsilon_{k+1} \end{cases}$$

$$f(x_k, a_k) = \begin{bmatrix} \left(s_0 + s_1 \cdot \theta_k + s_2 \cdot \theta_k^2\right) \cdot a_k \\ + s_3 \cdot e^{s_4 \cdot \theta_k} - s_5 \cdot \sin(\theta_k) \\ \dot{\theta}_k + \ddot{\theta}_k \cdot T \\ \theta_k + \dot{\theta}_k \cdot T \end{bmatrix}$$

$$h(x_k) = \begin{bmatrix} c_0^1 + c_1^1 \cdot \dot{\theta}_k + c_2^1 \cdot \theta_k + c_3^1 \cdot \dot{\theta}_k^2 \\ + c_4^1 \cdot \theta_k^2 + c_5^1 \cdot \dot{\theta}_k \cdot \theta_k \\ c_0^2 + c_1^2 \cdot \dot{\theta}_k + c_2^2 \cdot \theta_k + c_3^2 \cdot \dot{\theta}_k^2 \\ + c_4^2 \cdot \theta_k^2 + c_5^2 \cdot \dot{\theta}_k \cdot \theta_k \end{bmatrix} \tag{19}$$

where $x_k = [\ddot{\theta}_k \ \dot{\theta}_k \ \theta_k]^T$, $y_k = [y_k^1 \ y_k^2]^T$, and $a_k = a(k)$; ω_k and υ_k are the process noise and the measurement noise, respectively, which may involve the uncertainties caused by the model simplifications of (6)–(8), (18), etc.

Thus, (19), which consists of an open-loop equation describing the EMG-driven joint motion and a measure equation built on the EMG features, forms an EMG-based state-space model. With such a model, a normal prediction–correction approach such as the Kalman-type algorithm can be used to estimate the continuous joint movement from EMG signals, where the measurement equation is used to reject model uncertainties and external disturbances.

C. Rejection of the Influence Caused by External Load

The external load of the muscle/joint will influence the muscle activation and the EMG features. Although the uncertainty caused by the change of external load can be grouped into ω_k and υ_k of (19), its influence cannot be successfully rejected by the proposed measurement equations. This is because the EMG features, from which the measurement equations were built, are also influenced by the external load.

We still take the biceps brachii and the elbow joint as an example (see Fig. 2). The parameters involved in (19) can be identified by a set of EMG measurements with respect to a specific "reference external load." However, if this load changes, those parameters identified under this load will also change accordingly. We will show this by the experimental results in Section IV-B.

To overcome this problem, we propose a synthesized maximum normalization (*SMN*) algorithm. Here, we still use polynomials to synthesize the relationship between the maximum value of EMG and the external load, i.e.,

$$\psi(m) = \lambda_0 + \lambda_1 \cdot m + \lambda_2 \cdot m^2 + \lambda_3 \cdot m^3 \tag{20}$$

where m represents the weight of external load, ψ represents the maximum value of an EMG-relative state, such as $e(k)$, WL, or ZC, whereas the external weight is m, and λ_i $(i = 0, \ldots, 3)$ are constant coefficients.

The parameters in (20) can be identified by offline EMG data with respect to different loads. Then, the features can be normalized as

$$e^{\text{nor}}(k) = \frac{e(k)}{\psi_e(m)}, \ \text{WL}^{\text{nor}} = \frac{\text{WL}}{\psi_{\text{WL}}(m)}, \ \text{ZC}^{\text{nor}} = \frac{\text{ZC}}{\psi_{\text{ZC}}(m)}$$

where $\psi_e(m)$, $\psi_{\text{WL}}(m)$, and $\psi_{\text{ZC}}(m)$ are the maximum values of $e(k)$, WL, and ZC at the external load m, respectively.

D. Closed-Loop Motion Estimation

The parameters in (19), namely, γ_1, γ_2, A, s_i, and c_i^j $(i = 0, 1, \ldots, 5; j = 1, 2)$, can be identified offline first by a set of EMG measurements. Then, any nonlinear stochastic estimation algorithm can be used to estimate the joint motion via the parameterized reference model. In the following, we present the extended Kalman filter (EKF)-based approach as an example. The EKF has a closed-loop nature by use of the output injection term.

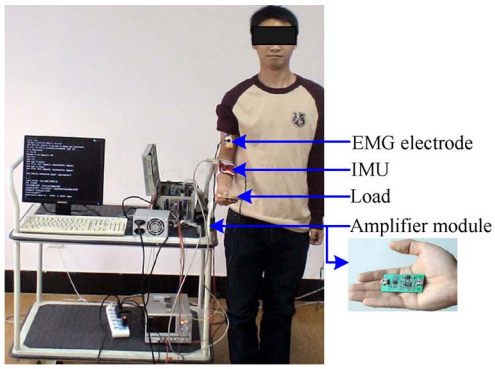

Fig. 3. Experimental setup.

To use the EKF algorithm, the nonlinear reference model of (19) is first linearized around the last estimated state by using Taylor series expansion, i.e.,

$$F_k = \frac{\partial f}{\partial x}\Big|_{x=\hat{x}_k} = \begin{bmatrix} 0 & 0 & (s_1 + 2\cdot s_2\cdot\theta_k)\cdot a_k \\ & & +\, s_3\cdot s_4\cdot e^{s_4\cdot\theta_k} - s_5\cdot\cos(\theta_k) \\ T & 1 & 0 \\ 0 & T & 1 \end{bmatrix} \tag{21}$$

$$H_{k+1} = \frac{\partial h}{\partial x}\Big|_{x=\hat{x}_{k+1,k}} = \begin{bmatrix} 0 & c_1^1 + 2\cdot c_3^1\cdot\dot{\theta}_k & c_2^1 + 2\cdot c_4^1\cdot\theta_k \\ & +\, c_5^1\cdot\theta_k & +c_5^1\cdot\dot{\theta}_k \\ 0 & c_1^2 + 2\cdot c_3^2\cdot\dot{\theta}_k & c_2^2 + 2\cdot c_4^2\cdot\theta_k \\ & +\, c_5^2\cdot\theta_k & +c_5^2\cdot\dot{\theta}_k \end{bmatrix}. \tag{22}$$

Then, the consecutive prediction–update cycle of the Kalman filter is used to propagate the minimum mean-square-error estimation [29].

Process Update

$$\begin{cases} \hat{x}_{k+1,k} = f(\hat{x}_k, a_k) \\ P_{k+1,k} = F_k\hat{x}_k F_k^T + Q \end{cases}. \tag{23}$$

Measurement Update

$$\begin{cases} K_{k+1} = P_{k+1,k}H_{k+1}^T\left(H_{k+1}P_{k+1,k}H_{k+1}^T + R\right)^{-1} \\ \hat{x}_{k+1} = \hat{x}_{k+1,k} + K_{k+1}\left(y_{k+1} - h(\hat{x}_{k+1,k})\right) \\ P_{k+1} = \left(I_{n\times n} - K_{k+1}H_{k+1}\right)P_{k+1,k} \end{cases}. \tag{24}$$

IV. Experiments

A. Experimental Setup

In order to verify the performance of the state-space EMG model and the normalization algorithm, an experimental scenario was set up, as shown in Fig. 3. In the experiments, the subject's surface skin of biceps brachii was first cleaned with alcohol; then, an active surface electrode (Triode, T3402M) was placed on the middle of biceps brachii to sample the EMG signals. For validating the model-based estimation, an IMU (VN-100) was also fixed on the forearm to record the "real" angular displacement and velocity of the elbow flexion/extension. Fig. 4 shows the positions of the sensors.

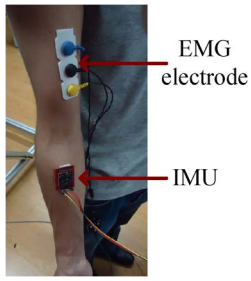

Fig. 4. Placements of the EMG electrode and the IMU.

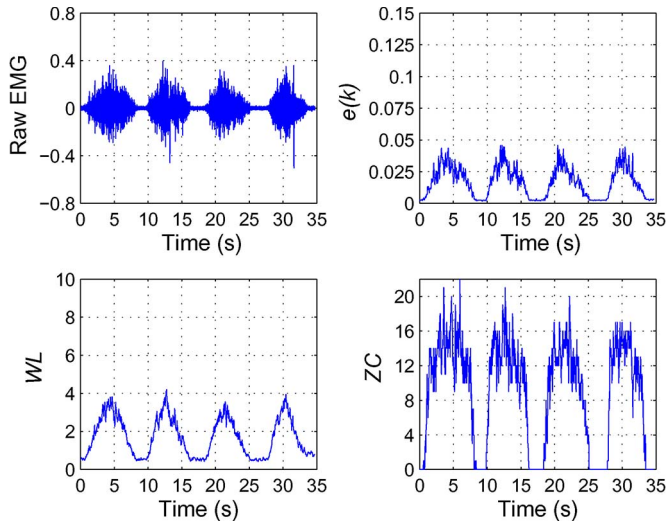

Fig. 5. Raw EMG signals and the EMG features with 1.54-kg load.

In the experiments, EMG signals were amplified by a circuit module (Myoscan) and then digitized by an analog-to-digital converter (PCI1716) with a sampling frequency of 1 kHz (sampling interval of 1 ms), and a 32-ms time window was set for extracting the EMG features. In total, three subjects were tested in our experiments (three males 27 ± 4 years old).

B. Experiment for Parameter Identification

The first experiment was to identify the unknown parameters in the EMG-driven model, i.e., γ_1, γ_2, A, s_i, and c_i^j $(i = 0, 1, \ldots 5; j = 1, 2)$ of (19), which was performed offline. Just like the one in Fig. 3, each of the three subjects flexed and extended his elbow with normal velocity $(5^\circ/\text{s} \sim 100^\circ/\text{s})$ to generate about 40 s of data. Then, the Levenberg–Marquardt algorithm [30] was used to identify the parameters while minimizing a defined cost function, i.e.,

$$\min\sqrt{\sum\left(z(\chi) - \hat{z}\right)^2} \tag{25}$$

where χ is an unknown parameter vector, z is the estimated value, and $\hat{z}$ is the IMU measurement value.

Two experiments were conducted with respect to two different handheld loads of 1.54 and 3.23 kg, respectively. Figs. 5 and 6 show the raw EMG signals, $e(k)$, WL, and ZC of Subject 1, for the handheld load of 1.54 and 3.23 kg, respectively. The identified values of Subject 1 are listed in Table I, from which we can see that the parameters shift due to different external

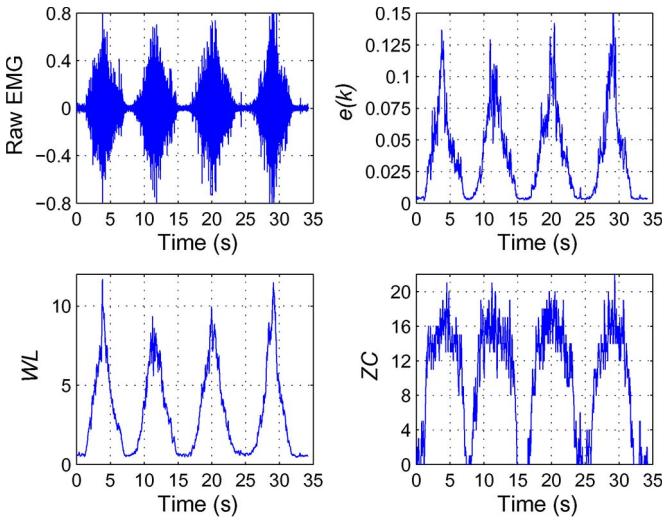

Fig. 6. Raw EMG signals and the EMG features with 3.23-kg load.

TABLE I
IDENTIFIED PARAMETERS WITH RESPECT TO DIFFERENT EXTERNAL LOADS USING MVC-BASED NORMALIZED ALGORITHM

load \ s_i	s_0	s_1	s_2	s_3	s_4	s_5
1.54kg	3.72	−5.58	−2.27	0.05	−0.49	0.34
3.23kg	1.69	−1.00	−0.19	0.13	−1.91	0.20
load \ c_i^1	c_0^1	c_1^1	c_2^1	c_3^1	c_4^1	c_5^1
1.54kg	−1.29	−0.01	2.66	−0.07	−0.73	0.10
3.23kg	−0.25	0.02	1.38	0.18	−0.22	0.28
load \ c_i^2	c_0^2	c_1^2	c_2^2	c_3^2	c_4^2	c_5^2
1.54kg	−4.22	0.23	8.56	0.15	−2.46	−0.11
3.23kg	−2.11	0.23	8.72	0.54	−2.40	−0.17

loads. The EMG-to-activation parameters not listed in Table I are the following: $\gamma_1 = 0.23$, $\gamma_2 = 0.28$, and $A = -1.78$; the same values are used for different loads.

In order to keep this paper brief, in the following, we will only present the detailed experimental results of Subject 1, whereas the other two subjects' results will be summarized in Section IV-E.

C. Experiment for State-Space Model Verification

By substituting the identified parameters into the state-space model of (19), we were able to use the EKF algorithm to estimate the motion states of the human arm only with the EMG measurements. In order to verify the improvement of the measurement equation, first, we used only the state equation of (14) to do the EKF-based estimation. Then, we used both the state and feedback equations of (19) to perform the same EKF estimation.

Fig. 7 shows the experimental results of the estimated joint angle and angular velocity at the load of 1.54 kg, where the IMU measurement serves as a "true" value for comparison.

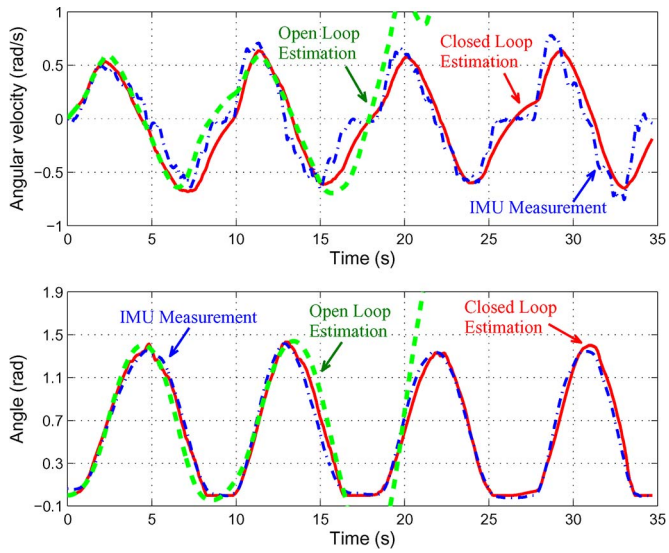

Fig. 7. Comparisons between the real and estimated motion: (blue) IMU measurement; (red) estimated value via state-space model (closed-loop estimation); (green) estimated value via open-loop model (open-loop estimation).

TABLE II
COMPARISONS BETWEEN IMU MEASUREMENT AND ESTIMATED VALUES

	$\Re_{vel}$(rad/s)	$\Re_{ang}$(rad)	ρ_{vel}	ρ_{ang}
IMU and open loop estimation	6.56	2.94	−0.20	0.28
IMU and closed loop estimation	0.15	0.10	0.91	0.99

From Fig. 7, we can see that the estimation based on the open-loop model diverged after 20 s due to the error accumulation. The proposed state-space model successfully overcame the error accumulation and kept the estimation convergent, while improving the estimation accuracy significantly.

In addition to the comparison in Fig. 7, we also propose two criteria to assess the estimation performance in quantity, i.e.,

$$\Re = \sqrt{\frac{1}{n}\cdot\sum_{i=1}^{n}(z_i-\hat{z}_i)^2} \quad \rho = \frac{C_{z\hat{z}}}{\sigma_z\cdot\sigma_{\hat{z}}} \tag{26}$$

where $\Re$ and ρ are the root mean-square-error (*RMSE*) and the correlation coefficient (*CC*), respectively; z represents the estimated value; $\hat{z}$ is the IMU measurement; n is the number of sample points; $C_{z\hat{z}}$ is the covariance coefficient; and σ_z and $\sigma_{\hat{z}}$ are the standard deviations.

Using the data in Fig. 7, we calculated the RMSE and the CC by (26) and listed the results in Table II. There are two rows in Table II:

- first row: the RMSE and the CC of both joint angle and angular velocity between IMU measurement and open-loop estimation;
- second row: the RMSE and the CC of both joint angle and angular velocity between IMU measurement and closed-loop estimation.

From Table II, we can see that the RMSEs of angle $(\Re_{\text{ang}})$ and angular velocity $(\Re_{\text{vel}})$ between the closed-loop estimation

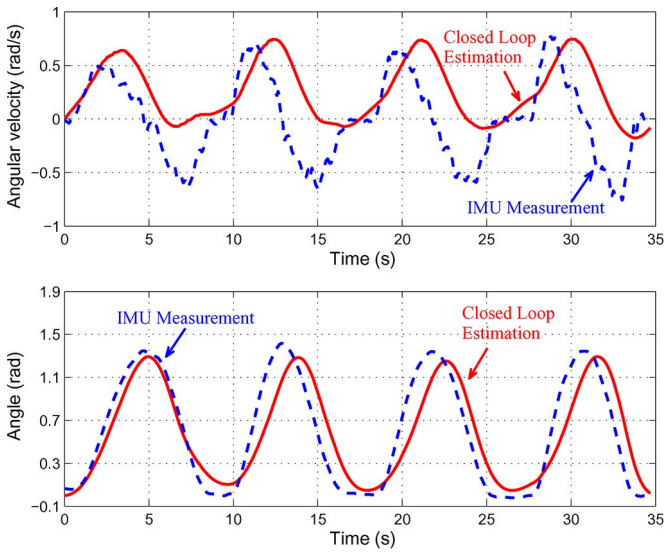

Fig. 8. Real and estimated motion while taking 1.54-kg load and using the reference model of 3.23-kg load, without SMN: (red) estimated value; (blue) IMU measurement.

and the IMU measurement are around 0.1 rad and 0.15 rad/s, respectively, which indicates that the errors between the real measurement and the estimation are relatively small. The two CC values, i.e., 0.99 and 0.91, are close to 1, which also indicates that the match between the estimation and the measurement is good. However, with respect to the estimation based on the open-loop model, due to the divergence after 20 s, both the RMSEs and the CCs indicate that the errors are much larger than those based on state-space model.

D. Experiment for External Disturbances Rejection

In Table I, we have already demonstrated the influence of external load to the parameters of the EMG model. Here, we first present what will happen to the EKF-based estimation if the reference model mismatches the actual condition. To do this, we used the reference model with the parameters identified at the load of 3.23 kg to estimate the motion states while the person holds a 1.54-kg load. Fig. 8 shows the experimental results, from which we can see that the uncertainty in the external load causes large deviation between the estimated and true values. The RMSE and CC values are also listed in the second row in Table V.

Then, we used the proposed SMN algorithm to normalize the EMG features. The subject (Subject 1) took nine different loads, respectively; and the corresponding maximum values of $e(k)$, WL, and ZC were obtained and shown in Fig. 9. The coefficients of three fitted polynomials are listed in Table III, and the synthesized curves are also shown in Fig. 9. We used the normalized EMG features to identify the model parameters with 3.23-kg load again, with the results being given in Table IV.

With the parameters in Table IV, we did the same EKF-based estimation by using (19), and the results were shown in Fig. 10. Comparison between Figs. 8 and 10 shows the improvement of the SMN. Additionally, for the estimated angular velocities and positions with and without SMN, the RMSE and the CC are given in Table V, from which we can see that the estimation

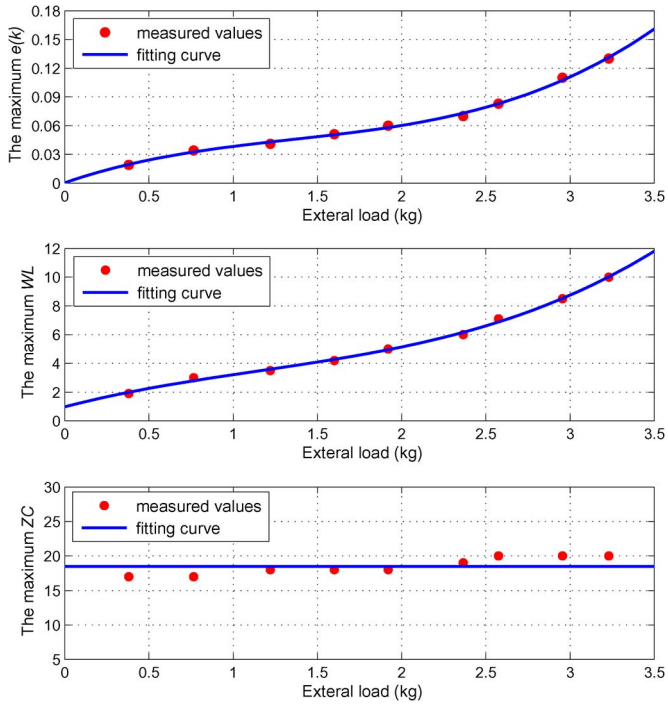

Fig. 9. Relationship between external loads and EMG-relative states.

TABLE III
COEFFICIENTS OF THE FITTING POLYNOMIALS FOR SMN

	λ_0	λ_1	λ_2	λ_3
ψ_e	0.0004	0.0609	−0.0304	0.0075
ψ_{WL}	0.9762	3.0585	−1.1525	0.3323
ψ_{ZC}	18	0	0	0

TABLE IV
IDENTIFIED PARAMETERS WITH RESPECT TO 3.23-kg EXTERNAL LOAD USING SMN ALGORITHM

s_0	s_1	s_2	s_3	s_4	s_5
1.09	−0.82	−0.24	0.11	−1.27	0.63
c_0^1	c_1^1	c_2^1	c_3^1	c_4^1	c_5^1
0.05	0.05	0.28	0.21	0.13	0.25
c_0^2	c_1^2	c_2^2	c_3^2	c_4^2	c_5^2
0.13	0.24	0.80	0.48	−0.26	−0.18

errors of RMSE are reduced to about 50% and the matches of CC are improved about 12.5%.

E. Experimental Results on the Other Two Subjects

Similar to that for Subject 1 (S#1), we also built the EMG-to-motion models for the other two subjects (S#2 and S#3) and calculated the RMSEs and the CCs by using their testing data. Corresponding to Tables II and V, the comparisons between

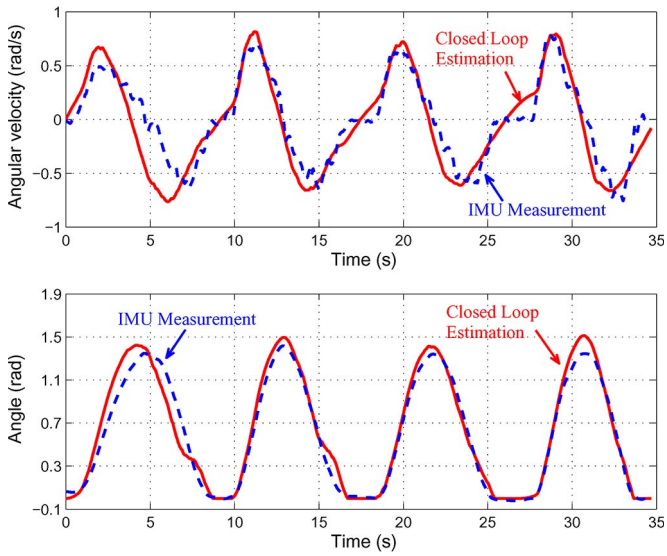

Fig. 10. Real and estimated motion while taking 1.54-kg load and using the reference model of 3.23-kg load, with SMN: (red) estimated value; (blue) IMU measurement.

TABLE V
COMPARISONS BETWEEN IMU MEASUREMENT AND ESTIMATED STATES WITH/WITHOUT SMN ALGORITHM

	$\Re_{vel}$(rad/s)	$\Re_{ang}$(rad)	ρ_{vel}	ρ_{ang}
with *SMN*	0.16	0.11	0.90	0.99
without *SMN*	0.40	0.24	0.61	0.88

TABLE VI
COMPARISONS BETWEEN IMU MEASUREMENT AND ESTIMATED VALUES OBTAINED BY OPEN-/CLOSED-LOOP ESTIMATION

		$\Re_{vel}$(rad/s)	$\Re_{ang}$(rad)	ρ_{vel}	ρ_{ang}
S#2	IMU and open loop estimation	5.68	2.13	0.09	0.33
	IMU and open loop estimation	0.16	0.12	0.89	0.97
S#3	IMU and open loop estimation	4.10	1.75	0.15	0.39
	IMU and open loop estimation	0.15	0.11	0.91	0.98

TABLE VII
COMPARISONS BETWEEN IMU MEASUREMENT AND ESTIMATED VALUES, WHILE THE SUBJECTS ARE TAKING 1.54-kg LOAD AND USING THE REFERENCE MODEL OF 3.23-kg LOAD

		$\Re_{vel}$(rad/s)	$\Re_{ang}$(rad)	ρ_{vel}	ρ_{ang}
S#2	with *SMN*	0.16	0.13	0.88	0.96
	without *SMN*	0.49	0.28	0.67	0.83
S#3	with *SMN*	0.16	0.11	0.89	0.97
	without *SMN*	0.31	0.19	0.77	0.89

IMU measurement and estimated values were listed in Tables VI and VII, from which we can get the similar conclusions as those for Subject 1.

V. CONCLUSION AND FUTURE WORK

In this paper, joint forward dynamics have been integrated into the normal HMM, and two EMG features have been employed to construct measurement equations, so that a state-space EMG model was built for continuous joint motion estimation. An improved normalization algorithm named synthesized maximum normalization was also proposed to reject the dependence of motion estimation on different external loads. Extensive experiments, as well as the comparisons between the model-based estimations and the IMU measurements, confirmed the effectiveness of the proposed methods.

In our future work, the proposed methods will be utilized to estimate the continuous motions of multiple joints by the EMG signals sampled from multiple muscles. The couplings among the EMG signals from different joint-relative muscles may introduce more challenging problems that could degrade the motion estimations of relative joints. In order to overcome the coupling problems, we are working on the Hill-based forward dynamics of multiple joints and the optimal selection and combination of EMG features for the construction of measurement equations. All the proposed algorithms will be also experimentally tested and compared with those corresponding to single joint in this paper.

REFERENCES

[1] Y. Oonishi, S. Oh, and Y. Hori, "A new control method for power-assisted wheelchair based on the surface myoelectric signal," *IEEE Trans. Ind. Electron.*, vol. 57, no. 9, pp. 3191–3196, Sep. 2010.
[2] Y. Nam, B. Koo, A. Cichocki, and S. Choi, "GOM-Face: GKP, EOG, EMG-based multimodal interface with application to humanoid robot control," *IEEE Trans. Biomed. Eng.*, vol. 61, no. 2, pp. 453–462, Feb. 2014.
[3] Y. Ueyama and E. Miyashita, "Optimal feedback control for predicting dynamic stiffness during arm movement," *IEEE Trans. Ind. Electron.*, vol. 61, no. 2, pp. 1044–1052, Feb. 2014.
[4] A. Gijsberts, M. Atzori, C. Castellini, H. Muller, and B. Caputo, "Movement error rate for evaluation of machine learning methods for sEMG-based hand movement classification," *IEEE Trans. Neural Syst. Rehabil. Eng.*, vol. 22, no. 4, pp. 735–744, Jul. 2014.
[5] R. H. Chowdhury *et al.*, "Surface electromyography signal processing and classification techniques," *Sensors*, vol. 13, no. 8, pp. 12 431–12 466, Sep. 2013.
[6] I. Mesa, A. Rubio, I. Tubia, J. De No, and J. Diaz, "Channel and feature selection for a surface electromyographic pattern recognition task," *Expert Syst. Appl.*, vol. 41, no. 11, pp. 5190–5200, Sep. 2014.
[7] L. J. Hargrove, G. Li, K. B. Englehart, and B. S. Hudgins, "Principal components analysis preprocessing for improved classification accuracies in pattern-recognition-based myoelectric control," *IEEE Trans. Biomed. Eng.*, vol. 56, no. 5, pp. 1407–1414, May 2009.
[8] A. Phinyomark, H. Hu, P. Phukpattaranont, and C. Limsakul, "Application of linear discriminant analysis in dimensionality reduction for hand motion classification," *Meas. Sci. Rev.*, vol. 12, no. 3, pp. 82–89, Jan. 2012.
[9] T. Matsubara and J. Morimoto, "Bilinear modeling of EMG signals to extract user-independent features for multiuser myoelectric interface," *IEEE Trans. Biomed. Eng.*, vol. 60, no. 8, pp. 2205–2213, Aug. 2013.
[10] N. Bu, M. Okamoto, and T. Tsuji, "A hybrid motion classification approach for EMG-based human–robot interfaces using Bayesian and neural networks," *IEEE Trans. Robot.*, vol. 25, no. 3, pp. 502–511, Jun. 2009.
[11] A. D. C. Chan and K. B. Englehart, "Continuous myoelectric control for powered prostheses using hidden Markov models," *IEEE Trans. Biomed. Eng.*, vol. 52, no. 1, pp. 121–124, Jan. 2005.
[12] Y. H. Huang, K. B. Englehart, B. Hudgins, and A. D. C. Chan, "A Gaussian mixture model based on classification scheme for myoelectric control of powered upper limb prostheses," *IEEE Trans. Biomed. Eng.*, vol. 52, no. 11, pp. 1801–1811, Nov. 2005.

[13] M. Khezri and M. Jahed, "A neuro-fuzzy inference system for sEMG-based identification of hand motion commands," *IEEE Trans. Ind. Electron.*, vol. 58, no. 5, pp. 1952–1960, May 2011.
[14] K. Kiguchi and Y. Hayashi, "An EMG-based control for an upper-limb power-assist exoskeleton robot," *IEEE Trans. Syst., Man, Cybern. B, Cybern.*, vol. 42, no. 4, pp. 1064–1071, Aug. 2012.
[15] R. Q. Lu, Z. J. Li, C. Y. Su, and A. Xue, "Development and learning control of a human limb with a rehabilitation exoskeleton," *IEEE Trans. Ind. Electron.*, vol. 61, no. 7, pp. 3776–3785, Jul. 2014.
[16] T. S. Buchanan, D. G. Lloyd, K. Manal, and T. F. Besier, "Neuromusculoskeletal modeling: Estimation of muscle forces and joint moments and movements from measurements of neural command," *J. Appl Biomech.*, vol. 20, no. 4, pp. 367–395, Nov. 2004.
[17] E. E. Cavallaro, J. Rosen, J. C. Perry, and S. Burns, "Real-time myoprocessors for a neural controlled powered exoskeleton arm," *IEEE Trans. Biomed. Eng.*, vol. 53, no. 11, pp. 1407–1414, Nov. 2006.
[18] C. Fleischer and G. Hommel, "A human–exoskeleton interface utilizing electromyography," *IEEE Trans. Robot.*, vol. 24, no. 4, pp. 872–882, Aug. 2008.
[19] M. Sartori, M. Reggiani, D. Farina, and D. G. Lloyd, "EMG-driven forward-dynamic estimation of muscle force and joint moment about multiple degrees of freedom in the human lower extremity," *PLoS One*, vol. 7, no. 12, pp. e52618-1–e52618-11, Dec. 2012.
[20] Q. Shao, D. N. Bassett, K. Manal, and T. S. Buchanan, "An EMG-driven model to estimate muscle forces and joint moments in stroke patients," *Comput. Biol Med.*, vol. 39, no. 12, pp. 1083–1088, Dec. 2009.
[21] D. G. Lloyd and T. E. Bessier, "An EMG-driven musculoskeletal model to estimate muscle forces and keen joint moments in vivo," *J. Biomech.*, vol. 36, no. 6, pp. 765–776, Jun. 2003.
[22] P. K. Artemiadis and K. J. Kyriakopoulos, "EMG-based control of a robot arm using low-dimensional embeddings," *IEEE Trans. Robot.*, vol. 26, no. 2, pp. 393–398, Apr. 2010.
[23] R. D. Woittiez, P. A. Huijing, H. B. Boom, and R. H. Rozendal, "A three-dimensional muscle model: A quantified relation between form and function of skeletal muscles," *J. Morphol.*, vol. 182, no. 1, pp. 95–113, Oct. 1984.
[24] Q. C. Ding, A. B. Xiong, X. G. Zhao, and J. D. Han, "A novel EMG-driven state space model for the estimation of continuous joint movements," in *Proc. IEEE SMC Conf.*, 2011, pp. 2891–2897.
[25] F. E. Zajac, "Muscle and tendon: Properties, models, scaling and application to biomechanics and motor control," *Crit. Rev. Biomed. Eng.*, vol. 17, no. 4, pp. 359–411, 1989.
[26] K. R. S. Holzbaur, W. M. Murray, and S. L. Delp, "A model of the upper extremity for simulating musculoskeletal surgery and analyzing neuromuscular control," *Ann. Biomed. Eng.*, vol. 33, no. 6, pp. 829–840, Jun. 2005.
[27] P. Pigeon, L. Yahia, and A. G. Feldman, "Moment arms and lengths of human upper limb muscles as functions of joint angles," *J. Biomech.*, vol. 29, no. 10, pp. 1365–1370, Oct. 1996.
[28] J. W. Ramsay, B. V. Hunter, and R. V. Gonzalez, "Muscle moment arm and normalized moment contributions as reference data for musculoskeletal elbow and wrist joint models," *J. Biomech.*, vol. 42, no. 4, pp. 463–473, Mar. 2009.
[29] F. Auger *et al.*, "Industrial applications of the Kalman filter: A review," *IEEE Trans. Ind. Electron.*, vol. 60, no. 12, pp. 5458–5471, Dec. 2013.
[30] J. Shawash and D. R. Selviah, "Real-time nonlinear parameter estimation using the Levenberg–Marquardt algorithm on field programmable gate arrays," *IEEE Trans. Ind. Electron.*, vol. 60, no. 1, pp. 170–176, Jan. 2013.

Jianda Han (M'05) received the Ph.D. degree in mechatronic engineering from Harbin Institute of Technology, Harbin, China, in 1998.

From 1998 to 2003, he was a Visiting Scientist with the City University of Hong Kong, Hong Kong; Michigan State University, East Lansing, MI, USA; and Cornell University, Ithaca, NY, USA. He is currently a Professor with the Shenyang Institute of Automation, Chinese Academy of Sciences, Shenyang, China, where he is also the Vice-Director of the State Key Laboratory of Robotics. His main research interests include enabling techniques and system integration of modular and wearable assistive robots and control for the autonomy of mobile robots.

Qichuan Ding received the B.E. degree in information and computing science from Shandong University, Jinan, China, in 2007. He is currently working toward the Ph.D. degree at the Shenyang Institute of Automation, Chinese Academy of Sciences, Shenyang, China.

He is also currently with the University of Chinese Academy of Sciences, Beijing, China. His main research interests include surface electromyography signal processing and pattern recognition.

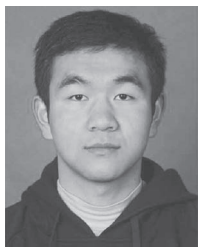

Anbin Xiong received the B.E. degree from Wuhan University of Technology, Wuhan, China, in 2009. He is currently working toward the Ph.D. degree at the Shenyang Institute of Automation, Chinese Academy of Sciences, Shenyang, China.

He is also currently with the University of Chinese Academy of Sciences, Beijing, China. His research interests include surface electromyography signal processing and control for rehabilitation robots.

Xingang Zhao (M'12) received the B.E. and M.E. degrees from Jilin University, Changchun, China, in 2000 and 2004, respectively, and the Ph.D. degree from the Chinese Academy of Sciences, Beijing, China, in 2008.

He is currently an Associate Professor with the Shenyang Institute of Automation, Chinese Academy of Sciences, Shenyang, China. His main research interests include medical robots, robot control, and pattern recognition.